Journal of Sound and Vibration (2000) **237**(4), 667–681
doi:10.1006/jsvi.2000.3042, available online at http://www.idealibrary.com on IDEAL®

A TIME-DOMAIN METHOD FOR DUCT ACOUSTICS

H. JU

Mechanical Engineering Department, The Hong Kong Polytechnic University, Hung Hom, Kowloon, Hong Kong, People's Republic of China. E-mail: mmkyfung@polyu.edu.hk

AND

K.-Y. FUNG

School of Power and Energy Engineering, Shanghai Jiao Tong University, Shanghai, People's Republic of China

(*Received* 15 *December* 1999, *and in final form* 28 *March* 2000)

This paper reports the development of a time-accurate method for prediction of acoustics in lined ducts. The multi-dimensional Euler equations are dimensionally split into a system of uni-directional simple wave equations, which are discretized and solved using an implicit compact high order finite-difference scheme. The split equations are closed and coupled through the concept of impedance at domain boundaries. Time-domain extensions of the impedance boundary condition and their efficient implementation are introduced for broadband and monotone waves. The method is benchmarked by the modal solution of a monopole in the lined duct, and used to investigate wall interference on the acoustic fields of realistic sources. Excellent agreement is found in the comparison with classical solutions, and the discrepancy found in the comparison with experiment is ascribable to experimental uncertainty.

1. INTRODUCTION

Duct acoustics is an area of continuous interest for its theoretical and practical importance. The increased requirement for quieter turbomachinery [1, 2], wind-tunnel testing environments [2–5], ventilation systems, public halls and transport tunnels [6] calls for a better understanding of the propagation of complex noise sources and effective techniques for their prediction and abatement under realistic conditions. Low-frequency acoustics in simple acoustically lined ducts or small enclosures of circular or rectangular cross-section without a mean flow is well understood and predicted through the classical theory of modal expansion [7–9]. Various methods, finite element, boundary element, and finite difference (FEM, BEM, FDM), have been employed to determine modal profiles when mean flow effects, temperature gradients, variable cross-sections, non-linear effects, arbitrary shapes, or acoustical treatments of ducts are considered [10–14].

For higher frequency, larger confinements, more complex liners or wall geometry, variable cross-sections, and realistic sources, the identification of the large amount of modes and modal profiles needed becomes increasingly difficult and ineffective [12]. Eversman and Baumeister [15] proposed a finite element model to simulate the acoustic field of a propeller in a circular wind tunnel with solid walls. Mosher developed a BEM model (panel method) to investigate wall effects on harmonic sources in an acoustically lined rectangular wind tunnel, but found substantial deviations between the predicted [4] and measured values [3] towards the tunnel walls where wall effects dominate. For low

0022-460X/00/440667 + 15 $35.00/0

absorption or low wave numbers, the model gave poor attenuation predictions, which were attributed to the inadequacy in the locally reactive impedance wall assumption used in the model. In addition, the formulation of frequency-domain methods such as BEM or FEM relies on the increasingly ineffective and inaccurate modal expansions for the implementation of a frequency-dependent, non-local radiation boundary condition for higher frequencies or larger confinements. Ray tracing is well established but only applicable for very high frequencies. For middle-frequency ranges in large enclosures such as a concert hall where wave behaviors are still dominant and a large number of modes are necessary, Botteldooren [16, 17] proposed a direct time-domain finite-difference approach.

Considering that many unsteady phenomena such as the shedding of vortices from a bluff body are impulsive in nature and their effects are often transient, local, and non-linear, the assumption of a harmonic field restricts the study of these phenomena. Time-domain methods have been developed for a wide range of flow conditions in the wind tunnel, addressing especially the effects of body geometry and flow non-linearity. These methods, however, often suffer from the added artificial damping and spurious dispersion for scheme stability and robustness, and their applications are primarily as a means towards steady or quasi-steady phenomena. A critical problem in their application to unsteady phenomena is the implementation of long-time stable, numerically accurate, and physically sound radiation and impedance boundary conditions. Baumeister [11] applied a second order time-domain finite-difference scheme to solve the wave equation, and remarked that a transient solver should need smaller storage for impedance boundaries than frequency-domain methods. Davis [18] introduced the low-dispersion finite-difference scheme for transient computation of acoustic pulses in a pipe with a time-equivalent impedance model for the open end. Botteldooren applied a second order leapfrog scheme on quasi-uniform rectangular grids with a simple time-equivalent impedance model to simulate low-frequency room acoustics [16, 17]. The treatment of realistic boundaries has been a critical issue for time-domain methods. Neither Davis nor Botteldooren addressed issues in their implementation of the impedance boundary condition. Tam and Auriault [19] pointed out the instability problem in the implementation of time-domain impedance-equivalent boundary conditions, and demonstrated the construction of stable impedance-dependent boundary schemes. Özyörük *et al.* [20] devised time-domain impedance operators via the z-transform and successfully applied their method to predict the decay of waves in a two-dimensional flow impedance tube. Reichert and Biringen [21] lumped the liner and bias flow effects as a source term in a time-domain duct model for application in noise suppression of jet engine nacelles. Selamet *et al.* [22] proposed a one-dimensional finite-difference scheme for non-linear acoustics and used it successfully for simulation of acoustic silencers.

Recently, Fung *et al.* [23] developed a new class of implicit, high order compact schemes for computation of waves. Their method reduces the linearized multi-dimensional Euler equations into a system of simple waves. In this formulation changes of pressure are shared among the modes and respective boundary conditions provide additional couplings. Not only can multi-dimensional problems be dimensionally split for efficient inversions, the implementation of realistic boundary conditions also benefits from the characteristics clarity in the split system. The robustness and accuracy of their approach have been demonstrated in a series of numerical experiments and benchmarking problems. The approach was further extended to include arbitrary geometry on rectilinear grids [24] and most recently time-domain impedance-equivalent boundary conditions [25].

We will outline in the following the formulation and discretization as a general approach to the three-dimensional aeroacoustics problem, discuss the implementation of time-domain impedance boundary conditions, and develop a method for prediction of wall

effects on the three-dimensional acoustic field of harmonic sources in lined ducts. The method will be benchmarked and its efficiency compared with an approximated analytic solution of modal expansion. Comparisons with the numerical and experimental results of Mosher [3, 4] will also be presented.

2. FORMULATION

For small disturbances in an inviscid, adiabatic flow the Euler equations can be separated into a part governing the steady homentropic mean flow:

$$\nabla\cdot(\rho_0\mathbf{U}_0) = 0, \qquad \rho_0\mathbf{U}_0\cdot\nabla\mathbf{U}_0 = -\nabla P_0, \tag{1}$$

and a part governing linear unsteady disturbances to first order:

$$\begin{aligned} &\frac{D_0}{Dt}\left(\frac{p}{\rho_0 C_0^2}\right) + \nabla\cdot\mathbf{u} + \mathbf{u}\cdot\nabla(\ln\rho_0) = \frac{1}{\rho_0} f_\rho, \\ &\frac{D_0\mathbf{u}}{Dt} + C_0^2\nabla\left(\frac{p}{\rho_0 C_0^2}\right) + \mathbf{u}\cdot\nabla\mathbf{U}_0 + \left(\frac{p}{\rho_0 C_0^2}\right)\nabla(C_0^2) = \frac{1}{\rho_0}\mathbf{f}. \end{aligned} \tag{2}$$

Here $D_0/Dt = \partial/\partial t + \mathbf{U}_0\cdot\nabla$ is the mean-flow convection derivative, $C_0 = \gamma P_0/\rho_0$ the mean sound speed, $\mathbf{U}_0 = (U_0, V_0, W_0)$, P_0, ρ_0, respectively, the mean velocity vector, pressure, and density; and $\mathbf{u} = (u, v, w)$, p, ρ their respective fluctuating quantities. The sources on the right-hand side include injection or expansion of fluids f_ρ and time-varying forces $\mathbf{f} = (f_x, f_y, f_z)$. When distance, speed and time are non-dimensionalized by the characteristic length L, reference sound speed C and L/C, respectively, pressure by $\rho_0 C_0^2$, fluctuating volume f_ρ by ρ_0, and fluctuating force $\mathbf{f}$ by $\rho_0 C^2/L$, equation (2) may assume hereinafter the dimensionless form

$$\frac{\partial U}{\partial t} + A_x\frac{\partial U}{\partial x} + A_y\frac{\partial U}{\partial y} + A_z\frac{\partial U}{\partial z} + (B_x + B_y + B_z)U = S \tag{3}$$

with

$$U = \begin{bmatrix} u \\ v \\ w \\ p \end{bmatrix}, \quad A_x = \begin{bmatrix} U_0 & 0 & 0 & C_0^2 \\ 0 & U_0 & 0 & 0 \\ 0 & 0 & U_0 & 0 \\ 1 & 0 & 0 & U_0 \end{bmatrix}, \quad A_y = \begin{bmatrix} V_0 & 0 & 0 & 0 \\ 0 & V_0 & 0 & C_0^2 \\ 0 & 0 & V_0 & 0 \\ 0 & 1 & 0 & V_0 \end{bmatrix},$$

$$A_z = \begin{bmatrix} W_0 & 0 & 0 & 0 \\ 0 & W_0 & 0 & 0 \\ 0 & 0 & W_0 & C_0^2 \\ 0 & 0 & 1 & W_0 \end{bmatrix},$$

$$B_x = \frac{\partial}{\partial x}\begin{bmatrix} U_0 & 0 & 0 & C_0^2 \\ V_0 & 0 & 0 & 0 \\ W_0 & 0 & 0 & 0 \\ \ln\rho_0 & 0 & 0 & 0 \end{bmatrix}, \quad B_y = \frac{\partial}{\partial y}\begin{bmatrix} 0 & U_0 & 0 & 0 \\ 0 & V_0 & 0 & C_0^2 \\ 0 & W_0 & 0 & 0 \\ 0 & \ln\rho_0 & 0 & 0 \end{bmatrix},$$

$$B_z = \frac{\partial}{\partial z}\begin{bmatrix} 0 & 0 & U_0 & 0 \\ 0 & 0 & V_0 & 0 \\ 0 & 0 & W_0 & C_0^2 \\ 0 & 0 & \ln\rho_0 & 0 \end{bmatrix},$$

and

$$S = \begin{bmatrix} f_x \\ f_y \\ f_z \\ f_\rho \end{bmatrix}.$$

Following Fung *et al.* [23], equation (3) is split into three equation sets:

$$\begin{aligned} &\frac{\partial U}{\partial t} + A_x\frac{\partial U}{\partial x} + \frac{1}{3}(B_x + B_y + B_z)U = \frac{1}{3}S, \\ &\frac{\partial U}{\partial t} + A_y\frac{\partial U}{\partial y} + \frac{1}{3}(B_x + B_y + B_z)U = \frac{1}{3}S, \\ &\frac{\partial U}{\partial t} + A_z\frac{\partial U}{\partial z} + \frac{1}{3}(B_x + B_y + B_z)U = \frac{1}{3}S, \end{aligned} \tag{4}$$

and

which can be solved in series and arbitrary order. This splitting may be understood from considering the contributions of the spatial variations $A_x\partial U/\partial x + A_y\partial U/\partial y + A_z\partial U/\partial z$ of equation (3) to the temporal advancement $\partial U/\partial t$. These contributions can be split into acoustic modes,

$$\begin{bmatrix} 0 & 0 & 0 & C_0^2 \\ 0 & 0 & 0 & 0 \\ 0 & 0 & 0 & 0 \\ 1 & 0 & 0 & 0 \end{bmatrix}\frac{\partial U}{\partial x} + \begin{bmatrix} 0 & 0 & 0 & 0 \\ 0 & 0 & 0 & C_0^2 \\ 0 & 0 & 0 & 0 \\ 0 & 1 & 0 & 0 \end{bmatrix}\frac{\partial U}{\partial y} + \begin{bmatrix} 0 & 0 & 0 & 0 \\ 0 & 0 & 0 & 0 \\ 0 & 0 & 0 & C_0^2 \\ 0 & 0 & 1 & 0 \end{bmatrix}\frac{\partial U}{\partial z},$$

and convective modes, $U_0\partial U/\partial x + V_0\partial U/\partial y + W_0\partial U/\partial z$. The contribution from the first row of the acoustic modes to the advancement of $u(x_j, n\Delta t) = u_j^n$, i.e., $\partial u/\partial t + C_0^2\,\partial p/\partial x = 0$, has no direct y- or z- dependence. Only the gradient of p_j^n in x affects the temporal advancement of u_j^n to u_j^{n+1}, and for which the coupling with the last row of the acoustic modes is needed. The advancement of p_j^n in the last row of the acoustic modes can be divided

into parts in the respective directions x, y, and z as

$$\frac{\partial p^*}{\partial t} + \frac{\partial u}{\partial x} = 0, \quad \frac{\partial p^{**}}{\partial t} + \frac{\partial v}{\partial y} = 0, \quad \frac{\partial p^{***}}{\partial t} + \frac{\partial w}{\partial z} = 0.$$

Therefore, the advancement of the acoustic modes in x involves only u_j^n and p_j^*; in y v_j^n and p_j^{**}; and in z w_j^n and in p_j^{***}. Pressure here acts as the coupling variable and is advanced in each direction regardless of the different notations p_j^*, p_j^{**}, and p_j^{***}, which are unnecessary when the most current value of p_j^* is used. However, the convective modes can simply be split into the directional convection equations:

$$\frac{\partial U}{\partial t} + U_0 \frac{\partial U}{\partial x} = 0, \quad \frac{\partial U}{\partial t} + V_0 \frac{\partial U}{\partial y} = 0, \quad \frac{\partial U}{\partial t} + W_0 \frac{\partial U}{\partial z} = 0,$$

and the linearity of equation (3) allows lumping of these separable directional effects into equation (4). Coupling may be strong when $(B_x + B_y + B_z)$ in equation (3) is a non-zero matrix, such as for acoustic refraction in a boundary layer where the mean flow $\mathbf{U}_0$ is non-uniform, or variations of C_0 and ρ_0 with temperature in a car muffler. The convenience of the split system should be weighted against the accuracy of the implementation, which is at worst first order in Δt if $(B_x + B_y + B_z)U_j^n$ is treated explicitly as a source. Other treatments of these source-like terms could improve the efficacy of the split system, but are beyond the scope of our consideration here.

It should be noted that this equation form, equation (4), known as fractional steps was advocated in pioneering works by Yanenko [26] and shown to be equivalent to the unsplit form for the simple wave equation. The difficulty was, however, in the implementation of numerically stable time-accurate physically meaningful boundary conditions through which effects from all variables are in various degrees coupled. Each directionally split set consists of four first order equations which are to be solved for the four variables subject to four spatial constraints to be imposed at the two ends in each direction of the solution domain. Appropriate specification of boundary condition becomes the critical issue. Ill-posed problems often imply solution instabilities, which can be suppressed by some form of damping changing effectively the order of the equations to second to allow specification of otherwise redundant boundary conditions. Damping has detrimental effects for waves, and must only be used when the effects are known and acceptable.

3. NUMERICAL SCHEME

Each equation set in equation (4) has the form $\partial U/\partial t + A_x \partial U/\partial x + \frac{1}{3}(B_x + B_y + B_z)U = \frac{1}{3}S$, which can be transformed into the quasi-characteristic equation,

$$\frac{\partial W_x}{\partial t} + \Lambda_x \frac{\partial W_x}{\partial x} = D_x U + \frac{1}{3} T_x S = S'.$$

Here, $\Lambda_x = \mathrm{diag}[\lambda_1, \lambda_2, \lambda_3, \lambda_4]$ (with $\lambda_{1,2} = U_0$ and $\lambda_{3,4} = U_0 \pm C_0$) are the characteristics (eigenvalues) of A_x, and $W_x = T_x U = [w_1, w_2, w_3, w_4]^{\mathrm{T}} = [v, w, u + p, u - p]^{\mathrm{T}}$ the principal modes (eigenvectors) through the transformation matrix $T_x (T_x A_x T_x^{-1} = \Lambda_x)$. Along the characteristic direction $\mathrm{d}x_i/\mathrm{d}t = \lambda_i$, the variation of w_i has a space–time causal relation, restricting the specification of boundary condition on w_i and the ways in which these equations can be advanced. The array $D_x = \Lambda_x \partial T_x/\partial x - \frac{1}{3} T_x (B_x + B_y + B_z)$ defines the coupling effects among the principal modes due to spatial variations in the mean

density, velocity, and temperature. The principal modes w_k, $k = 1$–4, are weakly coupled through $D_x U$, which is zero for a uniform mean flow and can be treated explicitly, depending on the accuracy requirement and degree of mean-flow non-uniformity.

Each principal mode $w_k(x, t)$ satisfies the common form

$$\frac{\partial w_k}{\partial t} + \lambda_k \frac{\partial w_k}{\partial x} = s'_k \tag{5}$$

of a simple wave, and the subscript k is simply dropped hereinafter for clarity. Let $w_j^n = w(x_j, n\Delta t)$ for a discrete set x_j in the x direction. A numerical scheme is to construct the coefficients a_j, b_j, c_j to advance w_j^n to w_j^{n+1}, i.e.,

$$\sum_{j=1, JN} a_j w_j^{n+1} = \sum_{j=1, JN} b_j w_j^n + \sum_{j=1, JN} c_j s_j'^{n+1/2}. \tag{6}$$

The choice of two solution levels, from n to $n + 1$, simplifies the data storage, but the resultant schemes are in general limited to second order accurate in Δt, although fourth order is achievable in special cases. If the three-point compact Padé approximation, $JN = 3$ in equation (6), is used for the spatial derivatives of equation (5) and the coefficients in equation (6) are chosen as those for the C3N of Fung *et al.* [23], the resultant tri-diagonal matrix can be easily solved using standard inversion routines.

For waves in particular, solution accuracy and stability also depend on the choice of coefficients and values of w_j^{n+1} for closure of equation (6) at the bounding points of a finite domain. A straightforward extrapolation of interior values to represent end values would lead to algorithmic instability. The sign of λ_k in equation (5) at a boundary determines the ways the coefficient matrix in equation (6) should be constructed. A positive eigenvalue λ_k implies that the corresponding wave w_k as a flow of information is moving from the left to the right boundary, and *vice versa*. Regardless of left or right, if from a direction inside the computational domain, w_k at a boundary point should be determined in such a way as not to have any immediate effect on the computation of the neighboring values, e.g., the characteristic method proposed in reference [23]. If from a direction outside of the computational domain, the value of w_k or a condition on this variable at a domain boundary must be given. The first two eigenvalues $\lambda_{1,2}$ in equation (5) correspond to convection of vortical disturbances. Their corresponding w_k should be prescribed as boundary values or obtained from the upstream interior. The other two correspond to acoustic modes, $[u + p, u - p]^{\mathrm{T}}$, which should be coupled at a physical or numerical boundary when $\lambda_{3,4}$ are of opposite signs. This type of boundary condition has been the most difficult to treat and the object of numerous studies. In the most general sense, the coupling between the two acoustic modes at a boundary can be characterized by the concept of impedance, whose forms and implementations will be discussed in the following section. If the characteristics of the acoustic modes at a boundary are of the same sign (supersonic, $U_0 > C_0$), again the presence of a boundary would have no consequence and the acoustic modes can be treated simply as convective effects with either given or extrapolated upstream values.

4. IMPEDANCE BOUNDARY CONDITIONS

The classical concept of impedance $Z(\omega) = \hat{p}/\hat{u}$ is a simplified model defined in the frequency domain (the arête denotes Fourier components with time factor $e^{i\omega t}$) to

characterize the reflection of plane harmonic waves from a wall. It has been demonstrated that a direct operational inversion of $Z(-\mathrm{i}\partial/\partial t)$ would, in general, result in unstable temporal operators [25], whereas the inversion of the corresponding reflection coefficient

$$\hat{W}(\omega) = \frac{1 - Z}{1 + Z}, \tag{7}$$

which relates the domain entering wave $\hat{u}^-$ (with the right boundary assumed) to the domain-exiting wave $\hat{u}^+$ as in $\hat{u}^- = \hat{W}(\omega)\hat{u}^+$ ($\hat{u}^\pm \equiv \hat{u} \pm \hat{p}$), corresponds to the stable time-convolution process

$$u^-(t) = \int_{-\infty}^{\infty} W(t - \tau)u^+(\tau)\,\mathrm{d}\tau.$$

Here $W(t)$ is the inverse Fourier transform of $\hat{W}(\omega)$, and is bounded by one as a bilinear mapping of all admissible Z with $\mathrm{Real}(Z) > 0$. The simple algebraic impedance model,

$$Z(\omega) = R + \mathrm{i}X(\omega) = R_0 + \mathrm{i}(X_{-1}/\omega + X_1\omega), \tag{8}$$

which describes a class of Helmholtz resonator-type sound absorptive materials of constant resistance, mass-like reactance at high frequencies, and spring-like reactance at low frequencies [7] is suitable for a discussion on the construction of time-domain impedance equivalent boundary conditions and sufficient to model reflections of harmonic waves. The algebraic form of equation (8) leads to the broadband reflection impulse:

$$W(t) = \tilde{W}(t)H(t) - \delta(t),$$

where

$$\tilde{W}(t) = \frac{2}{|X_1|}\sqrt{1 + \left(\frac{\omega_I}{\omega_R}\right)^2}\,\mathrm{e}^{-\omega_I t}\cos(\omega_R t + \chi), \quad \chi = \tan^{-1}\left(\frac{\omega_I}{\omega_R}\right),$$

$$\omega_R = \sqrt{\frac{-X_{-1}}{X_1} - \left(\frac{1 + R_0}{2X_1}\right)^2}, \quad \omega_I = \frac{1 + R_0}{2X_1},$$

$H(t)$ is the Heaviside function, and $\delta(t)$ the Dirac delta function. Thus, the reflected wave at the right boundary x_b is computed as

$$u^-(x_b, t) = \int_0^{\infty} W(\tau)u^+(x_b, t - \tau)\,\mathrm{d}\tau. \tag{9}$$

For the present applications, the restrictions $X_{-1}X_1 < 0$ (to allow positive and negative reactance values), $R_0 > 0$ (to ensure positive damping), and $-X_{-1}/X_1 \geqslant [(1 + R_0)/2X_1]^2$ are appropriate. These choices assure that only the past history of $u^+(x_b, t - \tau)$ ($\tau \geqslant 0$) up to the current time t determines the reflection, and the exponential decay in $\tilde{W}(t)$ determines the extent to which the history of $u^+(x_b, t - \tau)$ can be recorded. This pulse-like $\tilde{W}(t)$ oscillates at frequency ω_R as in $\cos(\omega_R t + \chi)$, decays exponentially at the rate of ω_I as in $\mathrm{e}^{-\omega_I t}$, and therefore only the localized reflection integral

$$u^-(x_b, t) = \int_0^{T_w} W(\tau)u^+(x_b, t - \tau)\,\mathrm{d}\tau \tag{10}$$

is needed for evaluation. The integration length T_w is inversely proportional to the decay of the imaginary part ω_I of the poles of $\hat{W}(\omega)$, and can be so chosen that $\tilde{W}(t) < \varepsilon$ for $t > T_w$ and any error bound ε. For single-frequency applications, only two parameters in model (8) are needed to represent the real and imaginary parts of a given impedance Z. The third one can be chosen to yield the minimum integration length

$$T_w = \frac{1}{|\omega_I|} \ln\left[\frac{2}{|X_1|\varepsilon}\sqrt{1+\left(\frac{\omega_I}{\omega_R}\right)^2}\right]$$

for a rapid convergence to the harmonic reflection. However, for materials with large ω_R, T_w should be large enough to assure integration smoothness of $\tilde{W}(t)$.

The implementation of equation (9) or equation (10) takes an efficient and simple form for impedances that have a set of simple roots ω_k for which $1 + Z(\omega_k) = 0$. We may assume for our purposes here that the imaginary part of ω_k is positive. Each of the roots then corresponds to the impedance impulse $e^{i\omega_k t}H(t)$, and equation (9) or equation (10) assumes the form

$$u^-(x_b, t) = \sum_k u_k^-(x_b, t),\ u_k^-(x_b, t) = \int_0^\infty e^{i\omega_k \tau} u^+(x_b, t-\tau)\,d\tau,$$

which can be approximated using the trapezoidal form of a z-transform with $z_k = e^{i\omega_k \Delta t}$ and the corresponding recursive boundary scheme:

$$u_k^-(x_b, t) = u^+(x_b, t)\frac{\Delta t}{2} + \sum_{j=1}^{n} z_k^j u^+(x_b, t - j\Delta t)\,\Delta t$$

$$= [u^+(x_b, t) + z_k u^+(x_b, t-\Delta t)]\frac{\Delta t}{2} + z_k u_k^-(x_b, t-\Delta t)$$

for the coupled acoustic modes in equation (5).

Since the formulation in the present method reduces the multi-dimensional Euler equations into a system of one-dimensional equations, the application of the boundary condition is the same as the one-dimensional case. In Cartesian co-ordinates the velocity in $u^\pm$ is simply the normal component, e.g., w on the grid plane x–y. The concept of impedance, or reflection coefficient, may also encompass other admissible boundary conditions for the Euler equations, including for solid wall $\hat{W} = -1$, for plane waves at the incident wave angle θ with a free-air boundary $\hat{W} = (\cos\theta - 1)/(1 + \cos\theta)$, and for the open ends of a duct $\hat{W} \approx 0$ as $\cos\theta \approx 1$.

5. POINT SOURCES

Sources in the present study are modeled as distributed ones for numerical smoothness. The following Gaussian distributed source has been shown effective in representing a monopole [27]:

$$f_\rho(r_s, t) = \frac{1}{W_h^3 \pi^{3/2}} e^{-(r_s/W_h)^2 + (kW_h)^2/4} \sin(\omega t), \tag{11}$$

where r_s is the distance from the source center at r_0, W_h the half-pulse width chosen to give a small but smooth distribution, k the wave number, and $e^{(kW_h)^2/4}$ the normalizing factor to

give an integrated source magnitude of unity. Similarly,

$$\mathbf{f}(r_s, t) = \frac{1}{W_h^3 \pi^{3/2}} \, \mathrm{e}^{-(r_s/W_h)^2 + (kW_h)^2/4} \sin(\omega t)\mathbf{n} \tag{12}$$

represents a point dipole of unit strength in the direction $\mathbf{n}$. The half-pulse-width to wavelength ratio $\bar{W}_h = W_h/\lambda$ for monopole representation can be a very small value ($\bar{W}_h = 0{\cdot}0751$ in this paper). A larger value is needed ($\bar{W}_h = 0{\cdot}2375$) for a dipole.

6. BENCHMARKING

We now demonstrate the effectiveness of the time-domain method for duct acoustics. For assessing the effects of wall interference on unsteady experiments in acoustically lined wind tunnels, Mosher [3] conducted acoustic measurement in a rectangular concrete duct with foam-lined side walls and anechoic end terminations, Figure 1. The inner dimensions of the duct are $240'' \times 46'' \times 94''$, with the radiation ends at $x = \{0, a\}$ and four impedance sidewalls at $y = \{0, b\}$ and $z = \{0, c\}$. Before comparing with experimental and other results, the present method is first benchmarked with the well-known modal solution of Morse and Ingard [7].

The pressure due to a monopole at (x_s, y_s, z_s) in the duct (Figure 1) is

$$\hat{p}(x, y, z, \omega) = \frac{\mathrm{i}\omega}{2S} \sum_{m,n=0}^{\infty} \frac{\Psi_{mn}(y, z)\Psi_{mn}(y_s, z_s)}{N_{ym} N_{zn} k_{mn}} \exp(\mathrm{i}k_{mn}|x - x_s|), \tag{13}$$

where

$$\Psi_{mn}(y, z) = Cs_m(q_m, y/b)Cs_n(q_n, z/c),\ Cs_m(q_m, y/b) = \begin{cases} \cos(\pi q_m y/b) & \text{for even } m, \\ \sin(\pi q_m y/b) & \text{for odd } m, \end{cases} \quad S = bc,$$

$$N_{ym} = \frac{1}{b}\int_{-b/2}^{b/2} Cs_m^2(q_m, y/b)\,\mathrm{d}y, \quad N_{zn} = \frac{1}{c}\int_{-c/2}^{c/2} Cs_n^2(q_n, z/c)\,\mathrm{d}y,$$

$$\text{and } k_{mn} = \sqrt{\omega^2 - \left(\frac{\pi m}{b}\right)^2 - \left(\frac{\pi n}{c}\right)^2}$$

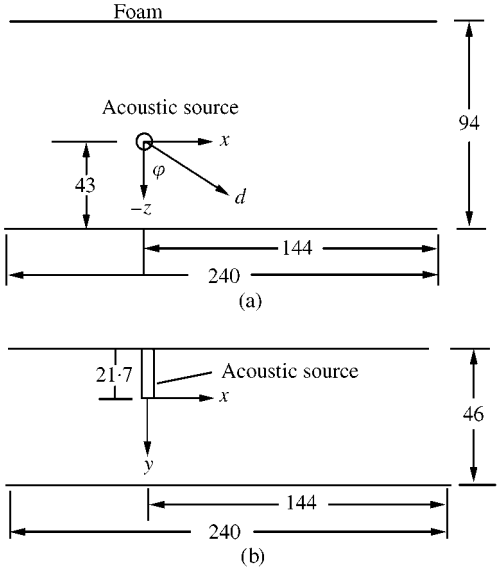

Figure 1. Duct geometry and dimensions in inches: (a) front view; (b) top view.

with a positive imaginary part. The wave numbers $q_m = -2ig_m$ are found by solving the wall constraint equations:

$$\begin{aligned} g_m \tanh(\pi g_m) &= ihe^{i\varphi} \quad \text{for even } m, \\ g_m \coth(\pi g_m) &= ihe^{i\varphi} \quad \text{for odd } m \end{aligned} \tag{14}$$

with $he^{i\varphi} = kb/(2\pi Z)$. The identification of eigenvalues q_m from equation (14) involves cumbersome iterative processes [8–10, 12, 28]. Here we solve the equivalent ordinary differential equations,

$$\frac{dg_m}{dh} = \begin{cases} \dfrac{ie^{i\varphi}\coth^2(\pi g_m)}{\sinh(\pi g_m)\coth(\pi g_m) + \pi g_m} & \text{for even } m, \\ \dfrac{ie^{i\varphi}\sinh^2(\pi g_m)}{\sinh(\pi g_m)\coth(\pi g_m) - \pi g_m} & \text{for odd } m \end{cases}$$

with initial values $q_0' = -i\sqrt{2ikb/(Z'\pi^2)}$, $q_m' = m - 2ikb/(mZ'\pi^2)$ for $m \neq 0$, and $|kb/Z'| \ll 1$.

Figure 2 shows a comparison of excess pressure defined as $20\log(4\pi\, d\hat{p}/k)$ in dB, in the duct over that in free air due to a monopole at $(x_s, y_s, z_s) = (96'', 20'', 42'')$. The variations

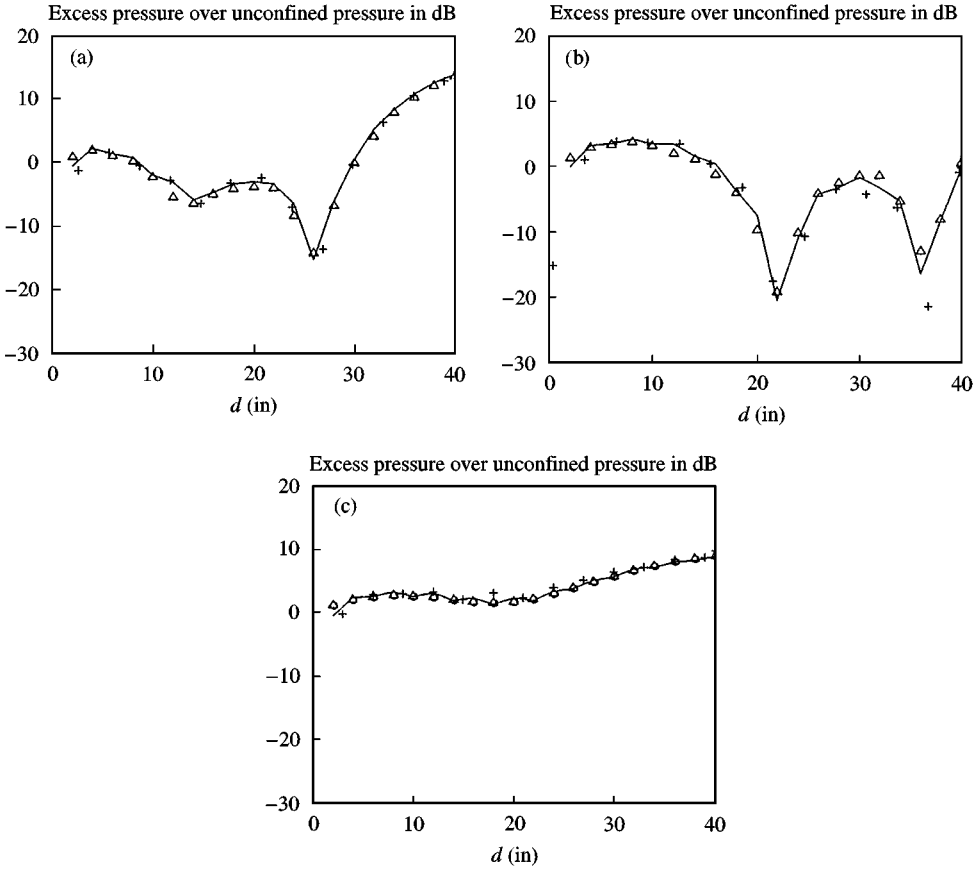

Figure 2. Comparison of predicted (——: $ppw \sim 25$, $+$: $ppw \sim 17$) and analytical (△: 453 modes in y and 1000 modes in z) excess pressure distributions for $f = 270{\cdot}38$ Hz and $Z = 1{\cdot}241 - 7{\cdot}27i$: (a) $\varphi' = 0°$; (b) $\varphi' = 180°$; (c) $\varphi' = 270°$.

with distance d from the source on the plane 1·0 inch in front of the source at angles $\varphi' = 0$, 180° and 270° (with respect to the negative z-axis, Figure 1) are shown, respectively, in Figures 2(a)–2(c). Excellent agreement with the modal solution is evident. A fine grid of 25 points per wavelength (*ppw*) in each co-ordinate was found to be amply adequate. A coarser grid of 17 *ppw* gave effectively the same results except near some nodes of the standing wave due to grid resolution. The modal solution at this frequency (270·38 Hz) was represented by 453 modes in y and up to 1000 modes in z, and took nearly 6 times longer to compute than that using the present time-domain method on the finer grid. The minimum numbers of modes for a solution accurate to 3 dB are 125 in y and 300 in z, for which the computing time is slightly more than that for the time-domain method.

7. WALL INTERFERENCE IN RECTANGULAR DUCT

In the experiment of Mosher [3], sound sources are modeled as the superposition of a monopole and a dipole in the y direction at $(x_s, y_s, z_s) = (96'', 21{\cdot}7'', 43'')$. The analytical pressure expression in free space (with time factor $e^{-i\omega t}$) is

$$\hat{p}(r, \varphi, \theta) = A_0 h_0(kr) + A_1 h_1(kr)\cos\theta,$$

where r is the distance from source to observer, θ the elevation angle with the $+y$-axis, φ the azimuth angle about the y-axis, and $h_n(kr)$ the nth order spherical Bessel function. The corresponding non-dimensional time-domain monopole and dipoles are

$$f_\rho = \text{Real}\left(\frac{4\pi A_0}{\omega k} e^{-i\omega t}\right), \quad f_x = f_z = 0, \quad f_y = \text{Real}\left(\frac{4\pi A_1}{ik^2} e^{-i\omega t}\right).$$

The experimental data given in Mosher [3] were normalized by the reference pressure near the source point and expressed in excess pressure in the duct over that in the anechoic chamber in dB. Only the relative magnitudes and phases between the two kinds of sources are relevant for comparison. Table 1 lists the source strengths and impedance values used in Mosher's two cases of study. The values listed in reference [3, p. 46] are for harmonic components of $e^{-i\omega t}$. They should correspond to reactance of the opposite sign for our computation here. However, when the original values were used, the computed attenuation of excess pressure (triangles in Figure 3) towards the open ends did not agree with the measured values (circles) but had similar behaviors as those (-- + --) predicted by Mosher. When the opposite sign was used, the agreement in both cases was excellent (solid line), suggesting an error in the published values.

TABLE 1

Cases of study

Frequency (Hz)	Wave number (1/m)	Specific impednace Z	Source strength
343·7	4·9428	1·241 − 7·27i	$A_0 = 0{\cdot}0216 + 0{\cdot}1519i$ $A_1 = 0{\cdot}0022 + 0{\cdot}0171i$
723·3	13·223	0·414 − 2·875i	$A_0 = 0{\cdot}1664 + 0{\cdot}3727i$ $A_1 = 0{\cdot}0098 + 0{\cdot}1109i$

Figures 3, 4(a) and 4(b) compare excess pressure distributions for the lower-frequency case. The results using the present method (solid lines) are in better agreement with the experiment (circles) than those computed by Mosher (-- + --). In the directions away from the source towards the tunnel ends (Figure 3), the pressure predicted by the present method agrees well with the measured values, whereas the panel method gives much lower magnitudes. Since the source is located 1·3 inches not symmetrically below the duct center axis, the variations toward the lower and upper walls (Figure 4(a) and 4(b)), are substantially different, showing a high degree of phase sensitivity. The predictions by the present method, albeit with some phase shift, give a much better agreement with the experiment than those of Mosher, which deviate in the opposite direction of the experiment and attenuate at a much faster rate towards the duct ends. Results for the higher frequency case (Figure 5) draw similar conclusions, notwithstanding Mosher's better agreement with the experiment.

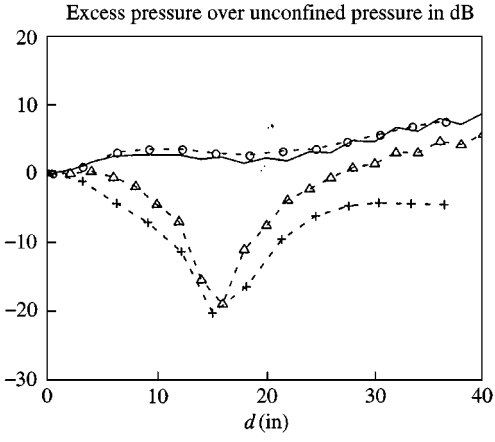

Figure 3. Comparison of predicted (—— presented method with $Z = 1{\cdot}241 - 7{\cdot}27\mathrm{i}$, --△-- present method with $Z = 1{\cdot}241 + 7{\cdot}27\mathrm{i}$, -- + -- panel method [3]) and measured [3] (--○--) excess pressure distributions for $f = 270{\cdot}38$ Hz and $\varphi' = 270°$.

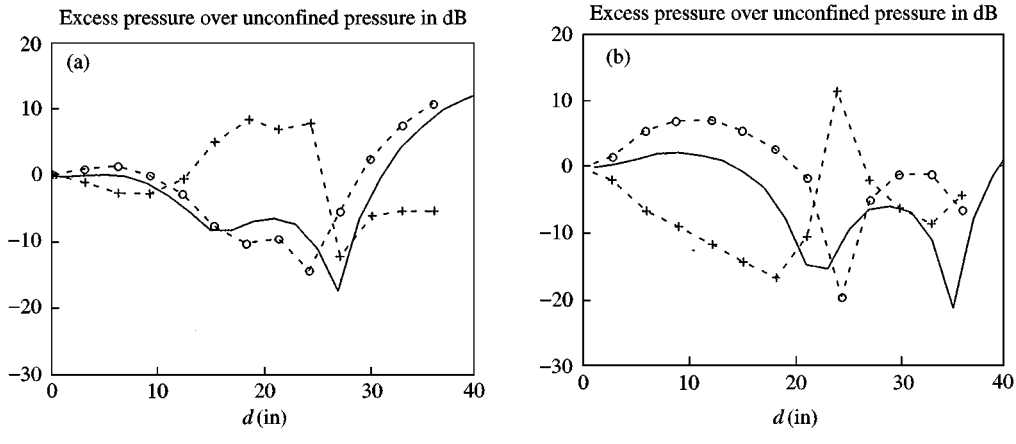

Figure 4. Comparison of predicted (——: presented method, -- + -- panel method [3]) and measured [3] (--○--) excess pressure distributions for $Z = 1{\cdot}241 - 7{\cdot}27\mathrm{i}$ and $f = 270{\cdot}38$ Hz: (a) $\varphi' = 0°$; (b) $\varphi' = 180°$.

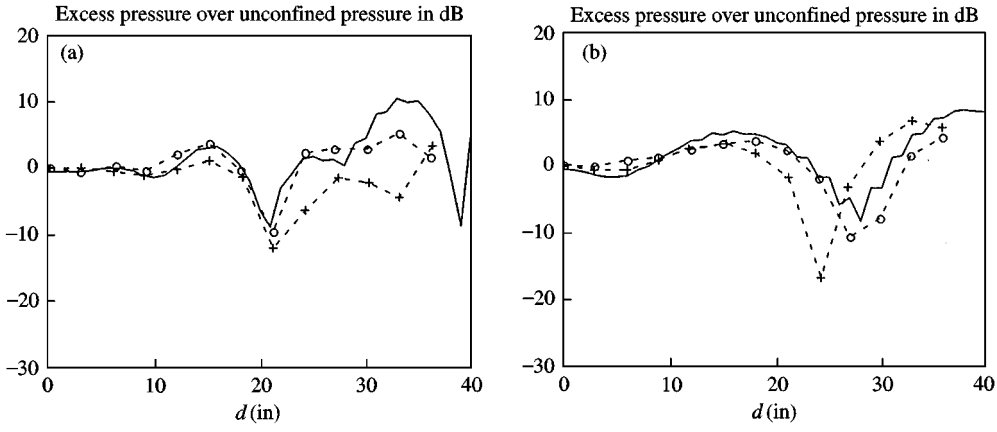

Figure 5. Comparison of predicted (——: presented method, -- + -- panel method [3]) and measured [3] (- - ○ - -) excess pressure distributions for $Z = 0{\cdot}414 - 2{\cdot}875\mathrm{i}$ and $f = 723{\cdot}34$ Hz: (a) $\varphi' = 0^\circ$; (b) $\varphi' = 90^\circ$.

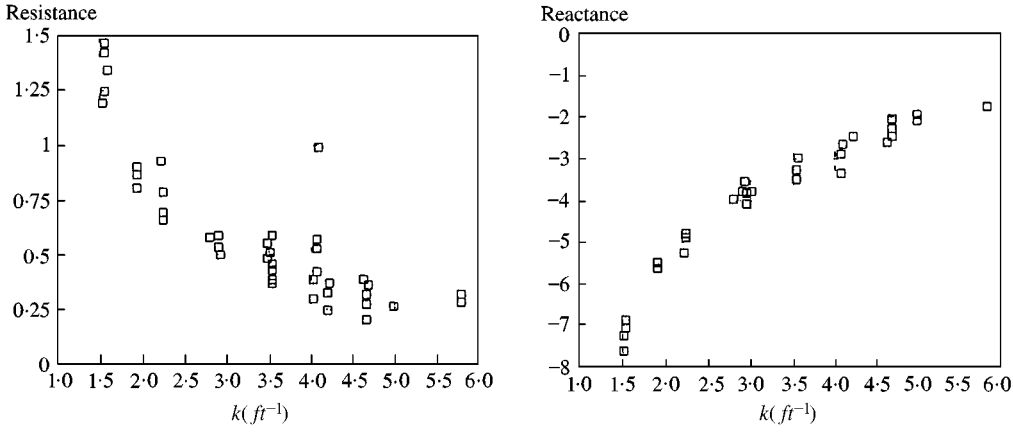

Figure 6. Measured impedance values in reference [3].

The tube-measured resistance and reactance data, Figure 6, for Mosher's experiment appear to have large ranges of experimental uncertainties at the wave numbers ($k = 1{\cdot}5065$ and $4{\cdot}0304$/ft) of the computed cases. The phase shifts found in Figures 4 and 5 between the measured and the present computed results are suspected to be due to the uncertainties in the tube-measured and *in situ* impedance values. Figure 7 illustrates margins of error in the computed excess pressure for the lower frequency using three slightly different impedance values $Z = 0{\cdot}8083 - 5{\cdot}8675\mathrm{i}$, $Z = 0{\cdot}7315 - 5{\cdot}5783\mathrm{i}$ and $Z = 0{\cdot}898 - 6{\cdot}1867\mathrm{i}$, corresponding, respectively, to reflection coefficients of $\hat{W} = 0{\cdot}9562\mathrm{e}^{\mathrm{i}161^\circ}$, $\hat{W} = 0{\cdot}9562\mathrm{e}^{\mathrm{i}160^\circ}$ and $\hat{W} = 0{\cdot}9562\mathrm{e}^{\mathrm{i}162^\circ}$. Merely $\pm 1^\circ$ phase variations in the reflection coefficients could account for over 10 dB changes near pressure nodes. The corresponding results at the higher frequency, Figure 8, with impedance values of $Z = 0{\cdot}414 - 2{\cdot}875\mathrm{i}$ ($\hat{W} = 0{\cdot}9158\mathrm{e}^{\mathrm{i}142{\cdot}3^\circ}$), $Z = 0{\cdot}3703 - 2{\cdot}7028\mathrm{i}$ ($\hat{W} = 0{\cdot}9158\mathrm{e}^{\mathrm{i}140^\circ}$) and $Z = 0{\cdot}452 - 3{\cdot}0165\mathrm{i}$ ($\hat{W} = 0{\cdot}9158\mathrm{e}^{\mathrm{i}144^\circ}$) show smaller ranges of uncertainties than at the lower frequency, which is consistent for the comparisons in Figures 4 and 5. The discrepancies may also be attributed to the locally reactive impedance assumption [3, 13], which is beyond the scope of the present study.

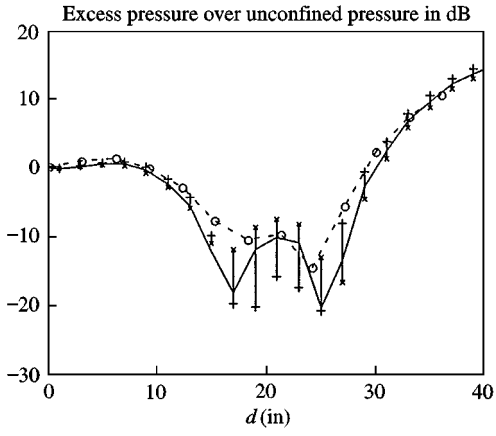

Figure 7. Comparison of predicted (—— $Z = 0{\cdot}8083 - 5{\cdot}8675i$, -- × -- $Z = 0{\cdot}898 - 6{\cdot}1867i$ and -- + -- $Z = 0{\cdot}7315 - 5{\cdot}5783i$) and measured [3] (- - ○ - -) excess pressure distributions for $f = 270{\cdot}38$ Hz and $\varphi' = 0°$.

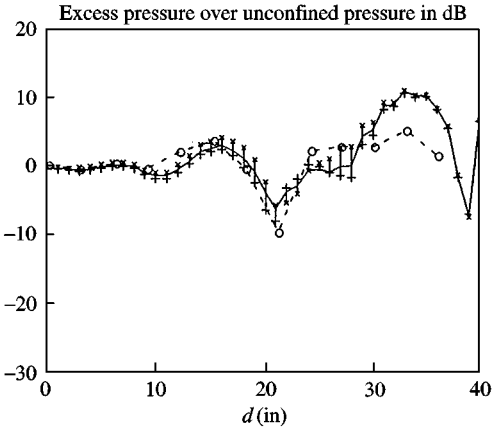

Figure 8. Comparison of predicted (—— $Z = 0{\cdot}414 - 2{\cdot}875i$, -- × -- $Z = 0{\cdot}3703 - 2{\cdot}7028i$ and -- + -- $Z = 0{\cdot}452 - 3{\cdot}0165i$) and measured [3] (- - ○ - -) excess pressure distributions for $f = 723{\cdot}34$ Hz and $\varphi' = 0°$.

8. CONCLUSIONS

An implicit time-domain compact scheme is proposed for studies and predictions of lined-duct acoustics. Time-domain impedance-equivalent conditions have been successfully implemented for all domain boundaries of a rectangular duct. The validity of the approach has been established by comparison with analytic solutions. The scheme has further been successfully applied for prediction of the interference of lined walls on the acoustic field of realistic sources. The computed fields using the present scheme are in good agreement with experiment, and are substantially better than those previously reported using the frequency-domain panel method. The phase shifts at low frequencies are ascribable to sensitivity of the near field to uncertainties in impedance.

REFERENCES

1. W. EVERSMAN 1995 *Theory and Practice, Vol. 2: Noise control* (H. H. Hubbard editor), 101–159. Acoustic Society of America. Theoretical models for duct acoustic propagation and radiation.
2. D. H. BUFFUM and S. FLEETER 1993 *ASME* 93-*GT*-149. Effect of wind tunnel acoustic modes on linear oscillating cascade aerodynamics.
3. M. MOSHER 1990 *NASA TM*-102801. Experimental validation study of an analytical model of discrete frequency sound propagation in closed-test-section wind tunnels.
4. M. MOSHER 1991 *Journal of the American Helicopter Society* **36**, 24–34. Low-frequency rotational noise in closed-test-section wind tunnels.
5. E. C. NASH, M. V. LOWSON and A. MCALPINE 1999 *Journal of Fluid Mechanics* **382**, 27–61. Boundary-layer instability noise on airfoils.
6. K. H. KUTTRUFF 1998 *Handbook of Acoustics* (M. J. Crocker editor), 925–938. New York: Wiley–Interscience Publication. Sound in enclosures.
7. P. M. MORSE and K. U. INGARD 1968 *Theoretical Acoustics*. New York: McGraw-Hill, Inc.
8. F. P. MECHEL 1991 *Acustica* **73**, 223–239. Modal solutions in rectangular ducts lined with locally reacting absorbers.
9. F. P. MECHEL 1998 *Acustica. Acta Acustica* **84**, 201–222. Modal solutions in circular and annular ducts with locally or bulk reacting lining.
10. A. H. NAYFEH, J. E. KAISER and D. P. TELIONIS 1975 *AIAA Journal* **13**, 130–153. Acoustics of aircraft engine-duct systems.
11. K. J. BAUMEISTER 1981 *Transactions of ASME, Journal of Engineering for Industry* **103**, 270–281. Numerical techniques in linear duct acoustics — a status report.
12. A. BIHHADI and Y. GERVAIS 1997 *Acustica* **83**, 1–12. Analysis of the distribution and attenuation of acoustic energy flux in lined duct containing inhomogeneous medium by the finite difference method.
13. C. Y. GLANDIER, C. E. FLOC'H and M. A. HAMDI 1997 *AIAA*-97-1686-*CP*. Analytical, numerical and experimental study of the acoustic behavior of a rectangular cavity with absorbing treatment on a wall.
14. W. H. LIN 1998 *Journal of Acoustical Society of America* **104**, 3111–3114. A least-squares spectral element method for sound propagation in acoustic ducts.
15. W. EVERSMAN and K. J. BAUMEISTER 1986 *Journal of Aircraft* **23**, 455–463. Modeling wind tunnel effects on the radiation characteristics of acoustic sources.
16. D. BOTTELDOOREN 1994 *Journal of Acoustical Society of America* **95**, 2313–2319. Acoustical finite-difference time-domain simulation in a quasi-Cartesian grid.
17. D. BOTTELDOOREN 1995 *Journal of Acoustical Society of America* **98**, 3302–3308. Finite-difference time-domain simulation of low-frequency room acoustic problems.
18. S. DAVIS 1991 *Journal of Acoustical Society of America* **90**, 2775–2781. Low-dispersion finite difference methods for acoustic waves in a pipe.
19. C. K. W. TAM and L. AURIAULT 1996 *AIAA Journal* **34**, 917–923. Time-domain impedance boundary conditions for computational acoustics.
20. Y. ÖZYÖRÜK, L. N. LONG and M. G. JONES 1998 *Journal of Computational Physics* **146**, 29–57. Time-domain numerical simulation of a flow-impedance tube.
21. R. S. REICHERT and S. BIRINGEN 1997 *AIAA*-97-1650. Time-domain simulation of acoustic propagation in a lined duct.
22. A. SELAMET, N. S. DICKEY and J. M. NOVAK 1995 *ASME Journal of Vibration and Acoustics* **117**, 323–331. A time-domain computational simulation of acoustic silencers.
23. K.-Y. FUNG, S. O. MAN and S. DAVIS 1996 *AIAA Journal* **34**, 2029–2037. An implicit high-order compact algorithm for computational acoustics.
24. K.-Y. FUNG 1997 *AIAA Paper* 97-1583. Development of compact wave solvers.
25. K.-Y. FUNG, H. B. JU and B. TALLAPRAGADA 2000 *AIAA Journal* **38**, 30–38. Impedance and its time-domain extensions.
26. N. N. YANENKO 1971 *The Method of Fractional Steps: the Solution of Problems of Mathematical Physics in Several Variables*. Berlin: Springer-Verlag.
27. H. B. JU and K.-Y. FUNG 1999 Time-domain simulation of acoustic sources over an impedance plane. (submitted for publication).
28. W. EVERSMAN 1975 *Journal of Sound and Vibration* **41**, 252–255. Computation of axial and transverse wave numbers for uniform two-dimensional ducts with flow using a numerical integration scheme.